HiSST: 2nd International Conference on
High-Speed Vehicle Science Technology
11–15 September 2022, Bruges, Belgium

CFD based interpolation of drag and heat rates of different objects re-entering the earth atmosphere in a prescribed motion.

P. Van Hauwaert[1], M. Spel[2], S. Galera[3], J. Annaloro[3], P. Omaly[3]

Abstract

Risk assessment of uncontrolled debris re-entering the atmosphere depends on various parameters among which drag and heat rates play a major role. However, those parameters cannot be computed with high fidelity methods such as CFD (Computational Fluid Dynamics) within a reasonable time frame for a full earth re-entry. Thus, correlations are usually used in spacecraft demise codes that use the object-oriented paradigm. However, correlations have often been derived in the 60s for non-destructive re-entry. In this paper, a new methodology to compute drag forces and heat rates for destructive re-entry in the continuum regime, for a large range of geometry is presented. The models are based on CFD computations. The method is applied to complex shape for implementation in the object-oriented code DEBRISK v3.

Keywords: *CFD, re-entry, random tumbling, Nondimensionalization, view-factor.*

Nomenclature

AoA – Angle of Attack
AoS – Angle of Side slip
ATT – attitude or couple (AoA, AoS)
BL – Blending
CD – Drag coefficient
CFD – Computational Fluid Dynamics
DSMC – Direct Simulation Monte Carlo
FC – Fully catalytic
K – Shape factor
LOO – Leave-One-Out
LPO – Leave-P-Out
NC – Non catalytic
NE – Non Equilibrium
PG – perfect gas
PV – « point de vol », see TP
Q – Flux, in Watt
QOI – Quantity of interest: K or CD
Req – Equivalent radius, in Meter
TP – Trajectory point.
Sadim – ratio between Sref and Souter/4 [-]
SM – Smallest scaled Median [m]
Souter – External surface of an object [m^2]
Sref – Reference surface [m^2]

1. Introduction

1.1. Presentation of the problem

Risk assessment of uncontrolled debris re-entering the atmosphere depends on various parameters among which drag and heat rates play a major role. However, they cannot be computed with high fidelity methods such as CFD within a reasonable time frame for a full earth re-entry. Thus, correlations are often used in object-oriented codes such as DEBRISK v2 [1], DRAMA v3 [2] or ORSAT [3]. However, models used in those codes have often been derived in the 60s for non-destructive re-entry based on [4]. And this methodology is only developed for one shape: the cylinder. Consequently, whenever a debris with a complex geometry needs to be modelled, an analogy is usually made with the cylinder.

[1] R.Tech, Amsterdam, The Netherlands, pierre@rtech-engineering.nl
[2] *R.Tech, Verniolle, France*
[3] *Centre National d'Etude Spatiales (CNES), France*

Copyright © 2022 by author(s)

This approach suffers from simplifying assumptions and results in large uncertainties on the survivability calculations. Moreover, [5] demonstrated those classical correlations underestimate the heat rates and overestimate the drag forces. And these correlations are available for a small range of geometries, actually sphere, cylinder, and parallelepiped (box, flat pate). The goal of this paper is to present a new methodology to compute efficiently drag and heat rates in the continuum regime, for a large range of geometries. The method is applied to complex shapes for implementing the correlations in the object-oriented code DEBRISK v3 [5].

1.2. Methodology

Debris are objects re-entering the atmosphere in an uncontrolled way. This means that object usually enters in a specific tumbling motion. The most common type of tumbling motion is the random tumbling. This means that in average the direction of the free-stream speed vector around the object is distributed uniformly and the drag and heat rate must be computed accordingly considering that uniform distribution of attitude. During a re-entry, the free-stream conditions vary because the altitude and the velocity of the object change. The wall temperature of the object changes due to aerothermal heating and the radiation cooling. And the geometry of the object changes because of the ablation process. As a result, the model must account for all these effects. The paper describes how to build such a model that can evaluate the tumbling average of both the drag force and the heat rate of an object re-entering the atmosphere in the continuum regime. The goal is to be able to compute the heat rates and drag force in random tumbling from:

- The free-stream conditions
- The wall temperature of the object
- The geometry parameters
- A database of non-dimensional parameters – named QOI (see section 1.4) for quantity of interest that characterize heat rate and drag force – that depends on the geometry. The variations of the non-dimensional parameters are small: the ratio between the maximum and the minimum is 2 for the heat rates and 1.25 for the drag forces.

The models are based on thousands of automated CFD computations. The initial goal was to create a database of CFD computations using an interpolation scheme. The main difficulties were to evaluate the different uncertainties associated with numerically simulation. In order for the CFD approach to be accurate while accounting for the variation described above, the following points are analyzed:

- The impact of the different CFD modellings (turbulence, catalycity, etc.) on the drag and heat rates is evaluated. A trade-off is made to select the CFD modelling to be used to run the computations with.
- The numerical convergence of each CFD computation is addressed. And the number of attitudes, thus number of CFD computations, required to model an average tumbling motion is evaluated.
- Normalization for a fix geometry: The effectiveness of the model that aims at reducing the dimensionality of the problem is demonstrated for a fix geometry. It involved variation with respect to the free-stream conditions and wall temperature. But normalization with respect to a homothetic shape is also verified.
- Normalization for different geometries: A further reduction of the variation of the QOIs (that represent drag and heat rates) over different geometries is demonstrated with careful choice of the geometric quantities: the equivalent radius and the reference surface. It results in small variations for the normalized parameters (the QOIs) to be used to compute the heat rate and drag. And it is important to minimized the variation with the geometry before the last step.
- Depending on the topology of the shape, a geometry can be modelled thought different parameters, for example a box can be defined by a length, a hight and a width. Depending on the aspect ratio of the shape, the value of the (normalized) QOIs can deviate from the average which is close to 1 in this work. A database that accounts for the variations of the

Copyright © 2022 by author(s)

QOIs and that depends on the geometry is generated for each shape. For a specific geometry, the QOIs are computed from the database using a multi-linear interpolation. In order for the interpolation to be accurate, the variation of the QOIs must be minimized thanks to the right choice of normalisation as well as the right choice of the parameters to account for the variation of the geometry. The database is created using CFD computations.

The complete methodology is applied for a class of complex shapes in the DEBRISK software. And the database is fed with more than 2000 CFDs.

One of the challenging aspects for the methodology to work is also described. It concerns the surface of reference selected which is the motion (random, end-over-end) average of the projected shape. A methodology applicable to geometries of arbitrary complexity to compute that quantity is presented.

1.3. Geometries

The geometries of interest shown in Fig. 1 are cylinder, tubes, cones, cone-segments and boxes of different dimensions and different aspect ratios. However, the methods presented are not specific to any on these shapes in particular. The differences that will be pointed out concern the type of tumbling and naturally the geometry quantities that differ from shape to shape. Moreover, CFDs on additional shapes such as spherical cap (e.g., Fig. 2) or segment of spherical cap (e.g., Fig. 5) have also been used to derive the model but results are not detailed here.

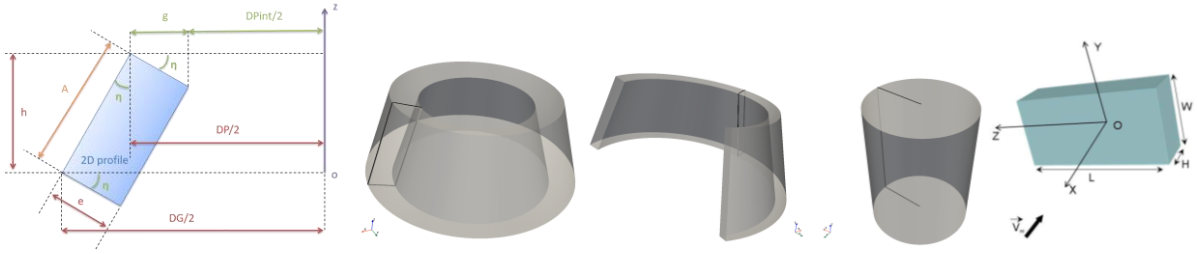

Fig. 1 : Definition of the geometry parameters and overview of the geometries. From left to right: 2D profile of a cone, cone, cone-segment, cylinder and box. Both a tube and a cylinder can be defined as a cone assuming η=0° or η=90

1.4. Definition of the quantity of interest or QOI

The model depends on the 2 QOIs or "Quantities of Interest", the drag coefficient "CD" defined by Eq. 1 and the shape factor "K" defined by Eq. 2. All comparisons are presented using only these 2 QOIs.

$$\mathrm{CD} = \frac{\overrightarrow{Force}.\frac{\overrightarrow{V_{inf}}}{\left|\overrightarrow{V_{inf}}\right|}}{\frac{1}{2}*\rho_{inf}*{V_{inf}}^{2}*S_{Ref}} \quad (1)$$

With:

- The reference surface in [m^2]: S_{Ref}
- The speed vector inflow for the current inflow condition in [m/s]: $\overrightarrow{V_{inf}}$
- The density for the current inflow condition in [kg/m^3]: ρ_{inf}
- The sum of the pressure and friction forces that apply on the object in [N]: $\overrightarrow{Force}$

$$\mathrm{K} = \frac{Q}{q_{adim\_HW}*S_{Ref}} \quad (2)$$

With:

- The reference surface in [m^2]: S_{Ref}
- The convective energy per unit of time received by the object, in [W]: Q
- A rate of energy per unit of area for hot wall, in [W/m^2]: q_{adim_HW}

Copyright © 2022 by author(s)

In the continuum regime q_{adim_HW} is computed through a DKR – Detra Kemp Riddel – formula [6] combined with a hot-wall correction:

$$q_{adim\_HW} = q_{stg} * HW_{corr} \tag{3}$$

With:

$$q_{stg} = \frac{1.10285e8}{\sqrt{Req}} * \sqrt{\frac{\rho_{inf}}{\rho_{sl}}} * (\frac{V_{inf}}{V_c})^{3.15} \tag{4}$$

Where:

- ρ_{sl} = 1.225 [kg/m^3]
- V_c = 7802.88 [m/s]

And With:

$$HW_{corr} = \frac{(h_{stg} - Cp(T_{wall}) * T_{wall})}{(h_{stg} - Cp(T_{ref}) * T_{ref})} \; if \; T_{wall} > T_{ref} \tag{5}$$

Or:

$$HW_{corr} = 1 \; if \; T_{wall} \leq T_{ref} \tag{6}$$

With:

$$h_{stg} = 0.5 \; * V * V + Cp * T \tag{7}$$

And:

- T_{ref}=300 [K]
- T_{wall}: the temperature at the wall.
- Cp : 1009 [J/K/kg]

Finally, in the reentry code, the drag force and the heat rate can be computed from CD, K, Req (the equivalent radius), Sref (the reference surface), the wall temperature and the local flow conditions. The goal of this paper is to describe a methodology to compute K, CD, Sref and Req so drag force and heat rate can be computed for an object re-entering the atmosphere with a tumbling motion.

1.5. Tumbling.

The QOI in tumbling depends on the tumbling mode. We assume it depends only on the topology of the geometry. While one can argue about the assumption made here, the conventions used in this work are:

- End-over-end tumbling for boxes. The axis of rotation matches the longest direction of the box.
- Random tumbling for all the other objects.

2. CFD Modeling

The CFD simulations have been carried out with Mistral-CFD [7]. Continuum regime and Mach number larger than 5 are of interest.

2.1. Mistral-CFD

Mistral-CFD has been developed at R.Tech since 2001. Various gas models can be run assuming either perfect gas, thermochemical equilibrium gas, or thermo-chemical nonequilibrium gas chemistry. While being originally developed for high-speed flows, it can handle flows from subsonic to hypersonic flows. An upwind finite volume method is used with an AUSM (Advection Upstream Splitting Method) derived inviscid flux scheme. The massively multi-blocked structured mesh approach allows flexibility in the geometrical modeling combined with efficient and accurate resolution of the physical phenomena. The

Copyright © 2022 by author(s)

large number of blocks makes also possible effective domain decomposition for parallelization on large scale computational facilities. The direct integration of the grid generator GridPro [8] allows the efficient creation of these massively multi-blocked grids.

The turbulent cases described in this work have been carried out with the SST (Shear Stress Transport) model of Menter. For chemical non equilibrium, the five species chemical reaction set air model of Dunn-Kang is used as it is a good compromise between computational time and accuracy. The "pseudo catalytic" model implemented in Mistral: the composition of the air defined as inflow is imposed at the wall. However, in the document it will be referred as "Fully catalytic" (FC) as it is considered to be a good approximation.
For some of the cases an unsteady flow has been observed, such as for the hollow sphere at angles around 30°. For those unsteady cases the heat fluxes and drag coefficients are time averaged over several periods.
In order to be able to automate the database generation, a single mesh is used for all flow angles. The outer boundary is spherical, with a diameter large enough to have a proper wake closure for all flow angles. High quality grids are produced using the GridPro grid generator [8].

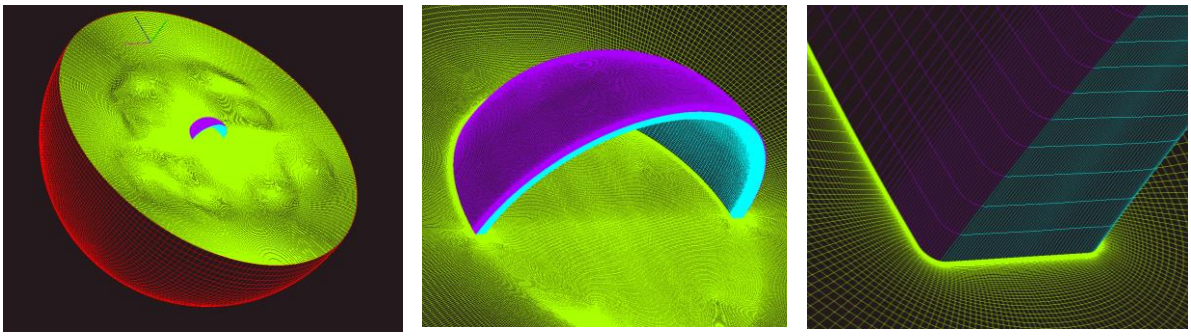

Fig. 2: Rotating mesh generated with GridPro.

2.2. CFD modeling

The tradeoff between different CFD modellings is twofold. It aims at selecting a numerical modelling before carrying out a large amount of CFD computations while keeping the amount of CPU time per computation under control. At the same time the uncertainties between the different modellings can be quantified. Relative values of both K and CD at fixed attitudes are compared. The inflow conditions used for the comparisons are listed in Table 5. The impact study includes:

- A comparison between perfect gas and non-equilibrium with FC
- A comparison between laminar flow and turbulent flow, both using perfect gas modeling
- The effect of catalycity

The majority of the comparisons have been carried out on a single shape: a cone-segment shown in Fig. 5 with the set of attitudes represented by colored points. The laminar flow with perfect gas – PG – modelling is used as "reference" for the comparison with the other modellings. It is compared with Non equilibrium – NE – modeling and FC wall, as well as with turbulent flow with PG modeling. This is presented in an attitude-to-attitude comparison, Fig. 3. A couple of Trajectory Points (TPs) – TP1 and TP2 – have been used. Table 1 sum up the trends for the tumbling coefficients.

The effect of using NE modeling with FC wall barely has any effects on the CD; but it reaches up to 10% in shape factor for some specific attitudes for the TP2 conditions. The effect on the QOI in tumbling (Table 1) can be up to 6% when considering TP2. The NE modelling has a small effect on both QOIs but the effect on the shape factor gets stronger as flow enthalpy increases.

The effect of using turbulent modelling is more significant as shown in Fig. 3 and Table 1. Local differences can be up to 50% on the shape factor and the difference for the tumbling shape factor range between 15% and 18%. Local effect on drag is less significant but the value in tumbling average differs of 4% with respect to the reference. The flow enthalpy does not strongly affect the comparison between the laminar and the turbulent modeling.

Copyright © 2022 by author(s)

While the QOI obtained with both GP modeling and NE with FC modeling are close, the effect of partial catalycity can play a major role. It depends on the TP, on the geometry, as well as on how much catalytic the wall is. Computation over sphere of different size and different TPs for a reentry trajectory have been carried out for both a fully catalytic (FC) wall and non-catalytic (NC) wall. While the result is not shown here, the conclusion is that it can reduce the integrated heat flux over a sphere such that a non-catalytic wall can only reach 60% of the heat rate computing with the FC assumption.

It has been decided to carry out the CFD simulations with the reference modeling: perfect gas, laminar flow based on the following conclusions:

- The reference results are very similar to the one obtained with NE modeling with FC wall.
- The laminar modeling is conservative with respect to the turbulent modeling for the shape factor in a context of risk assessment since the object is less likely to demise with a lower heat rate. It is the other way around for the drag coefficient since the turbulent modeling gives a higher drag, but the magnitude is lower. The issue of the trade-off between the two should be addressed in a context of a fully re-entry simulation however. Also, the transition between laminar and turbulent flow adds additional complexity that could be addressed afterward depending on specific reentry conditions.
- The computation costs for both the NE modeling and the turbulent modeling are about twice the computation costs of the PG laminar modeling.
- The partial catalytic effect can have a major impact on the shape factor and a NE modeling with NC wall is conservative in a context of risk assessment. However, an alternative approach is to model the partial catalytic effect as another step in the analytic formulation of the problem. The advantage is that it can also give flexibility in the catalycity modelling effect of the material. This is not discussed here.

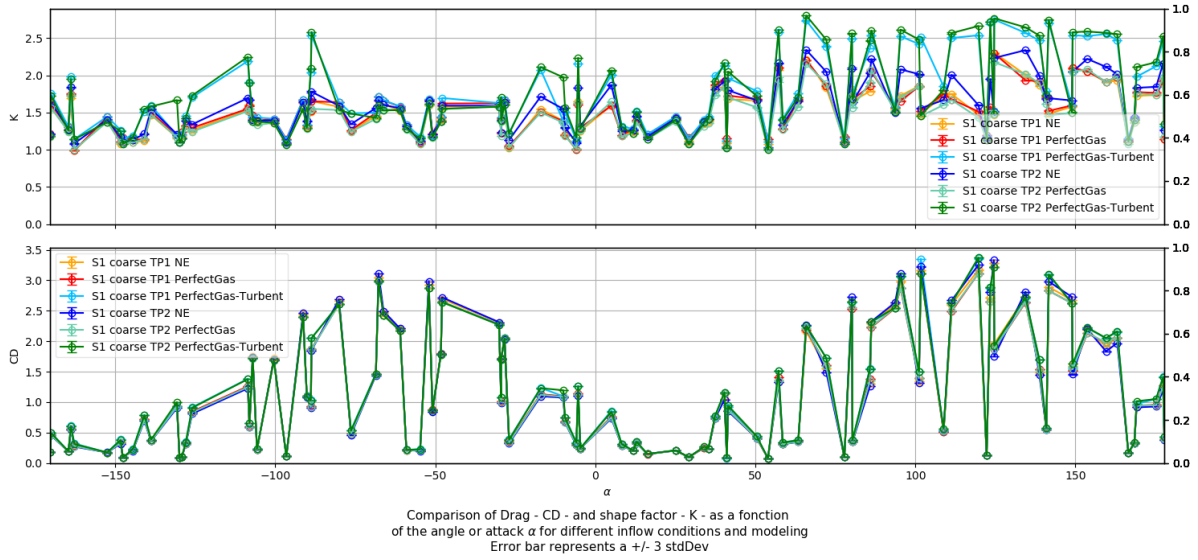

Fig. 3 : Comparison of the QOIs on a fix geometry for 100 attitudes with different numerical modellings and different inflow conditions. Only the variation in angle of attack is presented.

Copyright © 2022 by author(s)

Table 1 : Comparison of the QOI in tumbling on a fix geometry with different numerical modelling and different inflow condition – geometry cone-segment.

Condition	Modeling	CD	$(CD-CD_{PG})/CD_{PG}$	K	$(K-K_{PG})/K_{PG}$
TP1	PG	1.142	0	1.005	0
TP2	PG	1.139	0	0.975	0
TP1	PG-Turbulent	1.189	4.1%	1.158	15.2%
TP2	PG-Turbulent	1.189	4.3%	1.151	18.1%
TP1	NE	1.150	0.7%	0.990	-1.6%
TP2	NE	1.149	0.9%	1.038	6.5%

2.3. Numerical convergence

Different types of numerical convergence had to be taken care of. The time convergence of a CFD computation has been automated if the case was stationary. When it is was not, the computation is run in unsteady mode and both the average as well as the standard deviation are recovered such that a significant number of oscillations are accounted for. This methodology has been validated through an experimental rebuilding campaign at the VKI [9]. This methodology is needed since the average value can differs significantly from the instantaneous one for some attitudes as highlighted in Fig. 4.

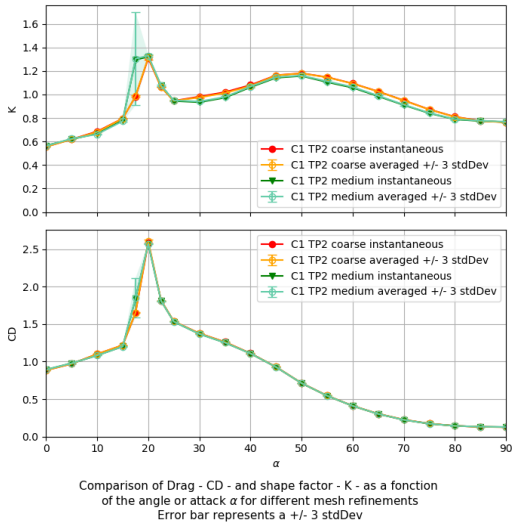

Fig. 4 : QOI as a function of the angle of attack for different mesh coarsening for shape C1.

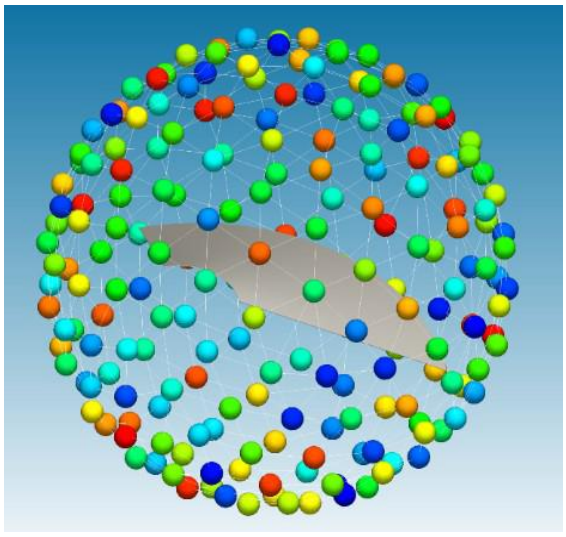

Fig. 5 : Distribution of attitudes for a shape (cone-segment) without any symmetry

The structured grids have been generated with the GridPro package. On top of having good grid quality, the advantage of the GridPro approach is that grid topologies can be reused on different geometries that have identical topology. Nevertheless, several grid levels are used to check grid convergence as presented in Fig. 4. Different grid levels named "coarse", "medium" and "fine" level are used with a 2^3 ratio for the number of cells between each of them. The grid convergence usually is more difficult in the area where unsteady behavior occurs.

The number of attitudes required to accurately compute the QOIs in tumbling depends on the type of tumbling motion, the shape and the symmetry. Two tumbling motions are considered: the "end-over-end" tumbling motion and the "random" tumbling motion. For a random tumbling motion, the number of attitudes to be consider can be reduced if the shape is axisymmetric and instead of a variation in

Copyright © 2022 by author(s)

{angle or attack, angle of sideslip}, only a variation in angle of attack has to be considered while accounting for the weight of each attitude appropriately. A study has been carried out for different shapes and number of attitudes. Eventually, the following number of attitudes were chosen:

- 50 attitudes for a shape without any symmetry
- 37 attitudes for an axisymmetric shape
- 19 attitudes for an axisymmetric shape and an additional plane of symmetry perpendicular to the axis of axisymmetric

A higher discretization in attitude is more beneficial to decrease the uncertainties over the drag coefficient rather than the those for the shape factor. This is because the variation in order of magnitude for the drag coefficient are larger than the ones for the shape factor when the attitude is varying as displayed Fig. 4. The additional average estimated error of choosing the upper-mentioned attitude discretization is 1% for the drag force and 1.6% for the shape factor. The maximum (over the geometry) estimated error is 3% for the drag force and 4% for the shape factor. Those errors are computed by comparing the QOI in tumbling for a specific number of attitudes and twice as much. The maximum error in drag coefficient is observed on cone while the maximum error in shape factor is observed on cone-segment.

These conclusions however exclude the half hollow sphere that exhibits very non-stationary behavior and it has been tackled differently [9].

3. Normalizations

The objective of the normalization is to have the values for the drag coefficient "CD" (Eq. 1) and for the shape factor "K" (Eq. 2) close to unity with the least variation. As it is presented in the last section, it aims at minimizing the interpolation errors and at improving the accuracy of the model. First, normalization with respect to the free-stream conditions and wall temperature is demonstrated. Then normalization across different geometries is looked at.

3.1. Inflow condition

The values for drag coefficient "CD" and for the shape factor "K" from Eq. 1 and Eq. 2 respectively, account for the inflow condition and for the wall temperature. For a fixed geometry, both QOIs stay more or less constant. This is sum up in Fig. 6 and Fig. 7 for the QOI in tumbling. Iso-CFD modelling has been used for both couples of inflow conditions. TP1/TP2 use perfect gas modelling and TP5/TP6 use NE. This observation of the QOI being more or less constant also is valid for most attitudes as shown in Fig. 8, Fig. 9 and also Fig. 3. Both QOIs differ near the location of the shock-shock interaction as shown Fig. 10 but the interaction happens at a different attitude depending on the TP. Significant differences in shape factor for all attitudes occur when decreasing in Mach number. This is illustrated Fig. 9 where TP8 (Mach5) is compared with other TPs. Some of the differences cancel each other out which eventually leads to similar QOI in tumbling as sum up in Table 2 for that particular case. Lower Mach number are of less interest because less ablation occurs then. Finally, it has been verified that scaling the geometry by 2 barely alters the results for the QOI as shown in Table 2.

Copyright © 2022 by author(s)

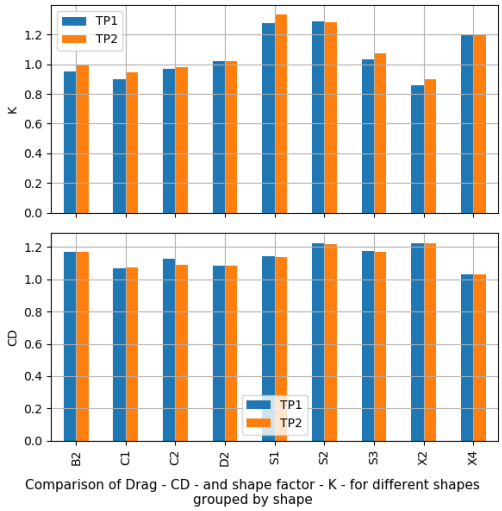

Fig. 6 : QOI in random tumbling for different inflow conditions for cones and cone-segments

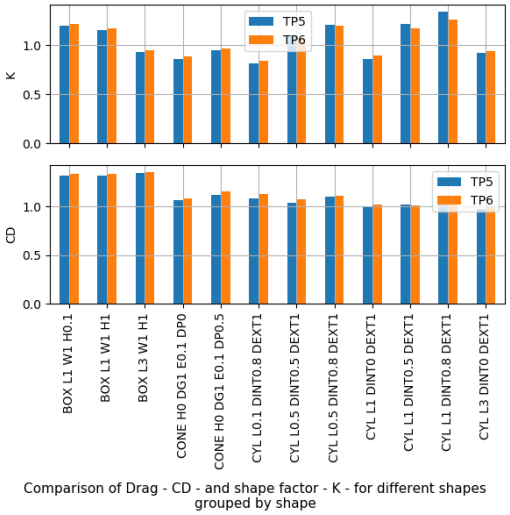

Fig. 7 : QOI in tumbling for different inflow conditions. The QOI for each box use end-over-end tumbling. The QOI for the other shapes use random tumbling.

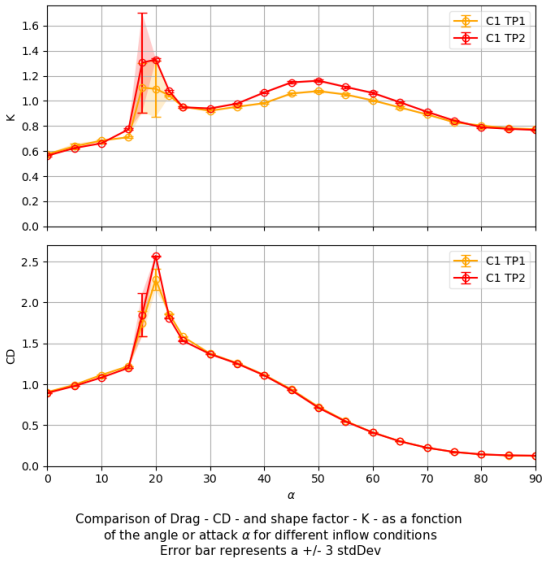

Fig. 8 : Comparison of the QOI for 2 different inflow conditions

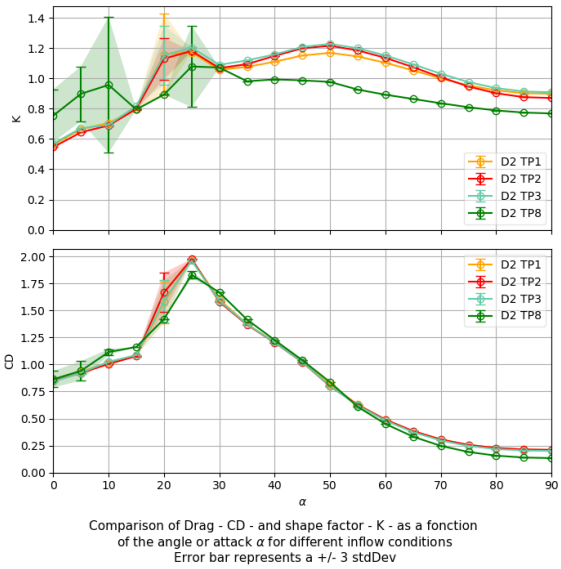

Fig. 9 Comparison of the QOI for 4 different inflow conditions for a "hollow tube"

Copyright © 2022 by author(s)

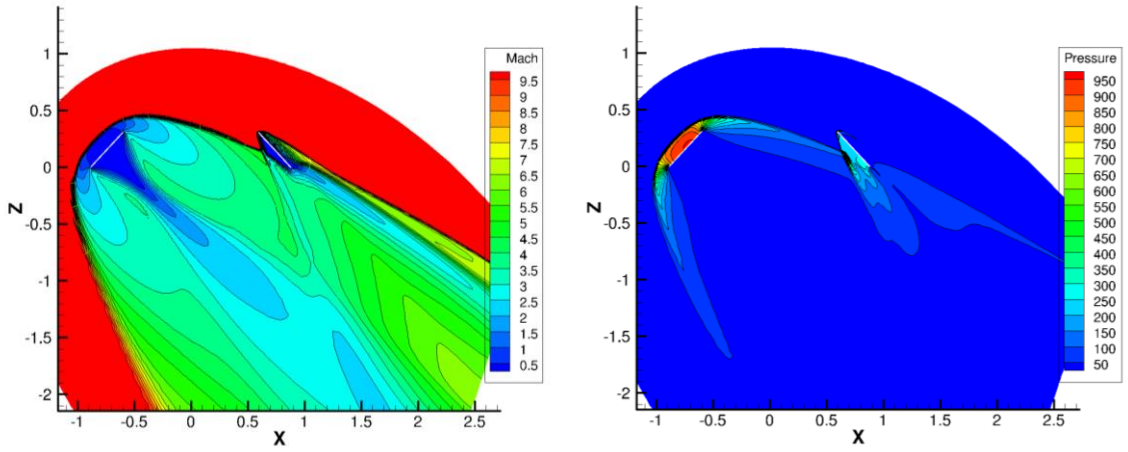

Fig. 10: Pressure and Mach number in the symmetry plane in a configuration with shock-shock interaction.

Table 2 : QOI in tumbling for different inflow condition for a fixed shape (D2, **Fig. 18**).

Scale	TP	Mach [-]	rho [kg/m3]	wall temperature [K]	CD	K
1	TP8	5	0.00384	1095	1.07	0.93
1	TP1	10	0.00011	1597	1.08	0.98
1	TP3	10	0.00011	799	1.07	1.01
1	TP2	15	8.6E-05	1095	1.08	0.99
2	TP1	10	0.00011	1597	1.05	0.97

3.2. Normalization of drag coefficient "CD" with the reference surface "Sref"

In order to normalize the drag coefficient between different geometries, the motion (random, end-over-end) average of the projected shape is selected as surface of reference (see section 4). It results in a narrow scattering of the CD for all shapes having a random tumbling motion as sum up Table 3. The ratio between the maximum and the minimum value over 41 shapes stays below 1.25. For end-over-end tumbling boxes the conclusion is similar but the average value is close to 1.3 as illustrated Fig. 7. Some selected results are given Table 7.

3.3. Normalization of shape factors "K" with the equivalent radius "Req"

The reference surface defined above is also used in Eq. 2 to compute the shape factor. The choice of an appropriate equivalent radius helps to normalize the shape factor. The equivalent radius chosen depends on the type of topology. One specific formulation is presented for each topology plus an additional one that can be applied for any shape. The selection of an equivalent radius has been done empirically. However, only simple formulation having easy-to-relate physical and geometry meaning have been considered.
For boxes, the second largest dimension of the box has been used to compute the results presented in Fig. 7. For cone, tube and cylinder, the "blending" – BL – have been used. Results are presented Fig. 13. Using the notation of Fig. 1, the definition of Req_{BL} is:

$$Req_{BL} = \left((1-\alpha_{BL}) * A + \alpha_{BL} * \frac{DG}{2}\right) * 1/\sqrt{2} \quad (8)$$

With:

Copyright © 2022 by author(s)

$$\alpha_{BL} = \frac{A}{A+DG} \tag{9}$$

This is a blending between a formulation that works well for a sub-category of cylinder and a formulation that works well for "rings", i.e., with DG >> A. This formulation is used for cylinders as well. Two different parametrizations for a profile of a cone can be used (see Fig. 1) to define a cylinder or a tube, but the one such as A>e is used.

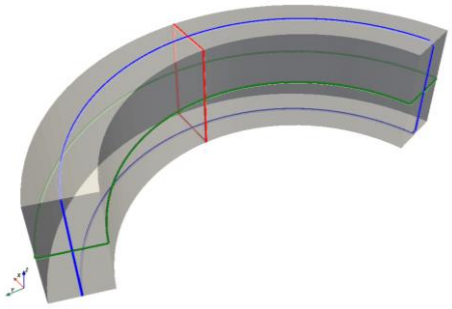

Fig. 11 : Cone-segment and its 3 medians lines in red, green and blue.

The other definition used for equivalent radius can be made general for various geometries. It is referred as "SM" for smallest scaled median. The idea is to draw the median line of the object (built from connecting the medians of the faces together), to take the smallest of them and to divide by $2 * \pi$ so it matches the sphere radius when the definition is applied to a sphere. An example for a cone-segment is presented Fig. 11 where Req_{SM} is the length of the red line divided by $2 * \pi$. The corresponding results for the cones, cylinder and tubes are presented Fig. 12. This formulation has some drawbacks when modelling some specific cylinders as a cone because one of the 2 following choices has to be made, both of which are not satisfactory:

- Assuming there is a continuity jump at DP=0.
- Assuming the median is going through the axis which is breaking the concept of using SM in the first place.

It is clear that the transition in geometry between a cylinder with a very small hole in place of its axis toward a tube with a larger hole that exhibits a complex shock-shock interaction structure is something that can only be quantified through CFD and for which a correlation model can only give an approximation. Table 3 sums up the limits of the analytical formula by giving the ratio of shape factor between the maximum and the minimum which does not go below two. In order to deal with the deviation of the QOIs for the normalized behavior, a database approach is described in the last section. Before that, the computation of the reference surface is addressed.

Table 3 : Statistical variation of the QOI for 41 selected cones, cylinders and cone-segments.

	CD	K, with Req=SM	K, with Req=BL
mean	1.09	0.663	1.042
std	0.06	0.136	0.177
min	0.98	0.471	0.702
max	1.22	1.051	1.407
max/min	1.24	2.231	2.004
std/mean	0.055	0.205	0.169

Copyright © 2022 by author(s)

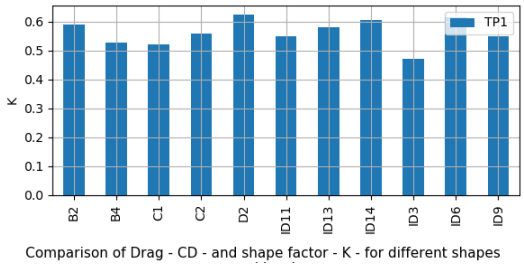

Fig. 12 : Shape factor in tumbling for cone, cylinder and cone-segment. Req=SM

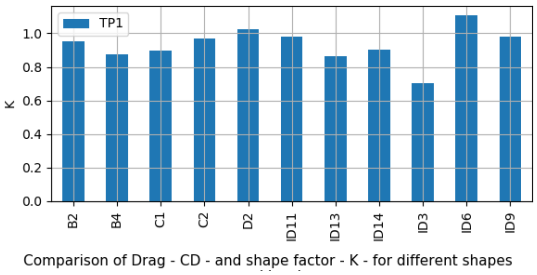

Fig. 13 : Shape factor in tumbling for cone, cylinder and cone-segment. Req=BL

4. Computation of Sref

The surface of reference selected is the motion (random, end-over-end) average of the projected shape. No general formulation is available to compute it analytically. A methodology that can be applied to any geometry that can be parameterized is presented. The idea is to compute it numerically from a surface mesh. But generating a triangular mesh and computing Sref numerically is costly – about a second in order magnitude – compared to a call to an analytic formulation. That is the reason the information is stored into a database so it can be called latter on, e.g., inside DEBRISK v3. The geometry is parameterized using non-dimensional parameters. For each set of parameters, "Sadim" is stored in the database so that the problem is non-dimensional:

$$Sadim = \frac{Sref}{Souter/4} \tag{10}$$

With "Souter" the area of the object.

This approach will work (in a reasonable amount of time) if:

- Geometries that can be parameterized by a small number or parameter, (e.g. 4), which mean a small database and small space of parameters to explore.
- "Sadim" is a continuous function and its variation are relatively smooth across the range of parameters considered to define the geometry.

After briefly describing the numerical method to compute Sref, the methodology and some results are presented.

4.1. Validation of the numerical code.

A C++/CUDA numerical code using ray tracing has been developed to carry out the task. Each ray is launched from the surface of the object toward a specific attitude. By counting the number of rays that intersect the surface, the projected surface can be computed. The accuracy depends on the number of rays as well as on the number of attitudes used. For convex shape in random tumbling, Cauchy [10] demonstrated in the 19th century that:

$$Sref = \frac{Souter}{4} \tag{11}$$

For some non-convex shape, it is possible to compute Sref analytically as well. The idea is to break down the surface into different primitive shapes and compute Sref using known view factor [11]. This method applied for tube (external radius "R", height "L" and thickness "e") gives:

$$Sref_{tube} = \frac{(S_{out}+S_{top}+S_{bot}+S_{in})}{4} \tag{12}$$

With:

$$S_{top} = S_{bot} = \pi(R^2 - (R-e)^2) \tag{13}$$

$$S_{top} = 2 * \pi * R * L \tag{14}$$

Copyright © 2022 by author(s)

$$S_{in} = \pi * (R - e) * L * (\sqrt{N^2 + 4} - N) \quad (15)$$

$$N = \frac{L}{R-e} \quad (16)$$

This formula has been used to validate the code. Variation of the aspect ratio of the tube across 4 orders of magnitude has been carried out and resulted in a maximum error contained below 1%. Additional cross checks is done with another much slower code. With the selected number of attitudes, number of triangles and number of rays per triangle, a computation with the C++/CUDA code takes about 2 seconds to run on a 2GFlops GPU.

4.2. Methodology to build the numerical database.

The following steps are carried out to build database:

- The geometry is parameterized using non-dimensional parameters, such as in Table 4.
- The boundaries of the domains of interest for computing Sref are defined. This is based on the expected use of the database. If the domain is very large, it is worth checking that below/above those limits Sadim will stays about constant, for example if blocking effects can be neglected in those area of the domain.
- Inside the boundaries of the domain, the numerical code is run on a discretized multidimensional Cartesian grid so that the accuracy required by the user is reached. An – Leave-P-Out (LPO) algorithm has been used to automatically discretize the domain where needed. This is illustrated in Fig. 14 for 2 non-dimensional parameters.
- Eventually the database can be used to compute Sref. The wanted value is computed through multi-linear interpolation. If the value is outside the domain of the database, the value corresponding to the closest point available is used instead (clipping). This is illustrated Fig. 16.

Table 4 : Non dimensional parameters used to parameterise cones and cone-segments.

Alias	Definition	meaning
L1	DPint/A	Internal diameter to apothem ratio
L2	e/A	Thickness to apothem ratio
L3	η	Half the angle of the cone
L4	θ	Angle of revolution around of the profile

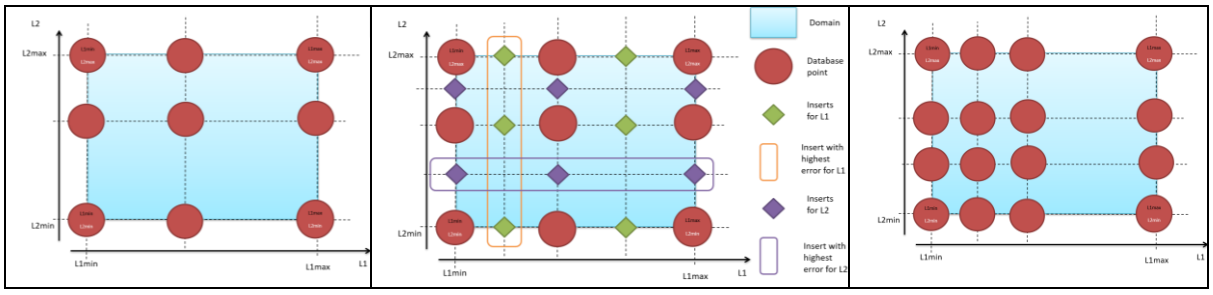

Fig. 14: LPO Algorithm for increasing Sref accuracy. Left: initial state of the database. Middle: evaluation of the best "inserts" to add inside the database. Right: state of the database after one iteration. Inserts are added only if the error is higher than a threshold.

4.3. Results

The methodology is applied to cone and cone-segment with the parameters defined Table 4 and the resulting discretization is presented Fig. 15 with a maximum error of 4% while the target error of 1%

Copyright © 2022 by author(s)

is achieved for most of the discretized space. The database contains about 100,000 points and can be stored for less than 1Mbytes in ASCII. It is interesting to note that for cones and cone-segments "Sadim" is bounded between 0.5 and 1. The methods have also been applied to spherical cap and segment of spherical cap with a maximum error of 1% and a smaller database. Finally, it is worth noting that "Sadim" is the view factor from the surface of the object to the "sky". Assuming the temperature of the object is uniform over all the surface, it can be used to model the effect of radiative cooling.

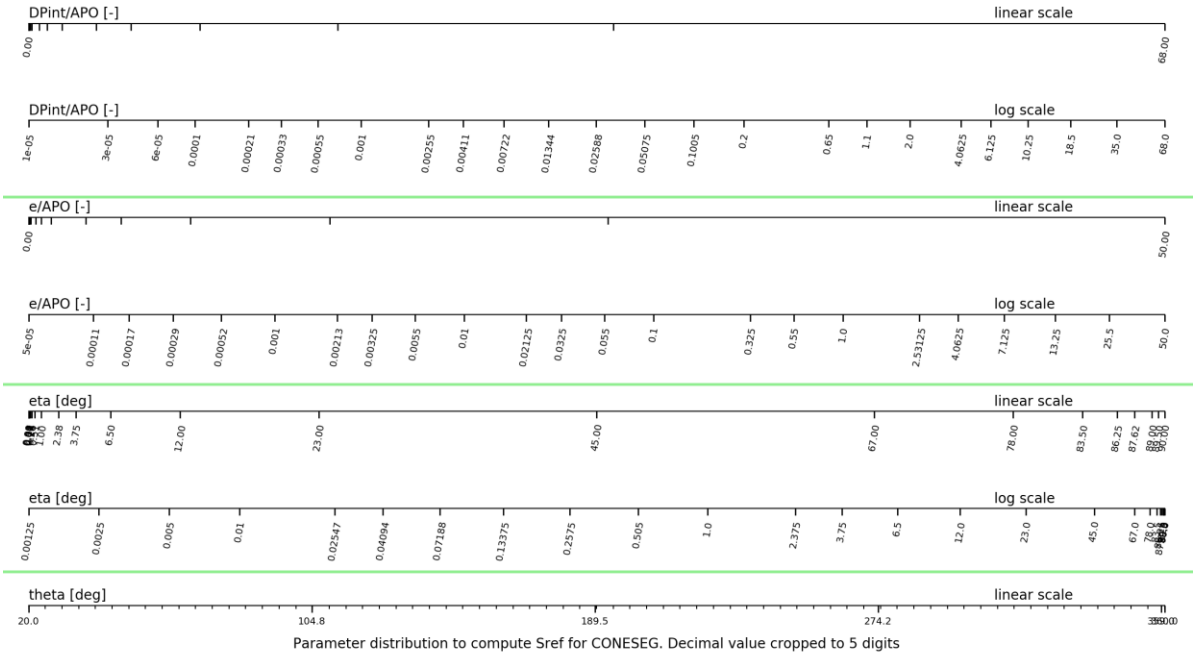

Fig. 15 : Non dimensional parameters used to parameterize cones and cone-segments

5. Application to DEBRISK

The methodology described in the previous sections has been applied for different geometries in the DEBRISK software [5], [9]. The DEBRISK software is briefly described, then the methodology is explained and some results are presented.

5.1. DEBRISK Software

In the frame of the French Space Operation Act (LOS) and in order to evaluate the risk on ground from debris generated by the atmospheric re-entry of space vehicles, CNES develops its own certification tool named DEBRISK. DEBRISK is based on an object-oriented approach. The main idea of this approach is to simplify the vehicle geometry from the break-up altitude into individual simple shapes, defined by the user. The trajectory, the thermal heat load and the possible ablation processes are computed for each fragment. Finally, the demise altitude or the casualty area (in case of survivability) is provided. This type of code must be able to simulate the full atmospheric reentry for hundred debris or more within minutes; the calculation time is therefore an important factor in the context of model development. The methodology must therefore be as accurate as possible in the assessment of QOI while still being fast.

5.2. Methodology

An interpolation model based on multi-linear interpolation of the QOIs from a database depending on the aspect ratio of complex shapes is helping to deal with the deviation of the QOIs from the normalized behaviour described previously. This database is fed with more than 2000 CFD computations. The methodology is based on the construction of databases similarly to what is done in section 4.2 but K and CD are used instead of Sadim. Also, the non-dimensional geometry parameters can be different. Another difference is that the databases are refined locally with single CFD matrices. The following steps are carried out for each geometry class in order to generate the database:

Copyright © 2022 by author(s)

- A bounding box "BB" of non-dimensional parameters that defined the geometry of interest has to be specified. This can be done using aspect ratio between various lengths of the object or with angles. Additional point – i.e. geometry – can be added inside the BB in order to locally increase the accuracy of the database. The absolute dimensions of the geometry do not matter as long as the Navier-Stokes equations stay valid for the combination of geometry and TP chosen for the computation.
- For every single geometry point:
    - A CFD matrix of different attitudes corresponding to the tumbling mode and the symmetry of the geometry is run.
    - The 2 QOIs – CD and K – are computed from the drag force and the heat rates of the CFD computations.
    - Non dimensional parameters are computed for the geometry of interest. They are named L_i, so (L_1, L_2) for a 2-dimensionnal database.
- Two databases, one for CD and one for K, are filled for all geometries using the data from the previous step, see Fig. 16. The missing point (green diamond) at computed though interpolation.

Once the two databases is created, they can be used with the formula Eq. 1 and Eq. 2 to evaluate the drag force and the heat rate for a couple {geometry, TP}:

- The non-dimensional geometry parameters L_i are computed from the geometry definition
- L_i are used to look up for an approximation of K and CD in the database. This is illustrated in Fig. 16. A multi-linear interpolation is used.
- The drag forces and heat rates are computed from Eq. 1 and Eq. 2 respectively.

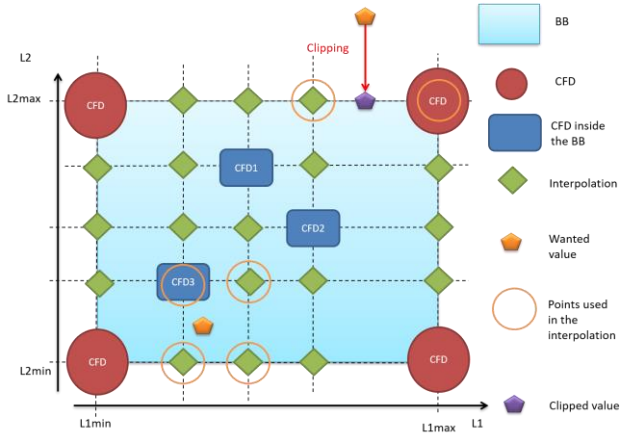

Fig. 16 : Illustration of the QOI look up in a 2-dimensionnal database

5.3. Results.

The methodology has been applied for boxes, cylinder and as well as more complex shapes such as cones. The CFD database has been built iteratively using ablation trajectory generated from DEBRISK with a large number of objects. The area of interest where to carry out the next CFD matrices were defined using those trajectories as well as the existing CFD points. Convergence of the method was evaluated through series of Leave-one-out (LOO). Fig. 17 is showing one of them for some selected data taken from Table 7. The rest of the CFD data used to construct database and carry out the LOO cannot be given for confidentiality reason. Nevertheless, Fig. 17 shows that the trends for both QOI are correctly captured. Req_{BL} is showing a lower error than Req_{SM} for the selected data. It is worth noting that the LOO carried out on the full set of CFD (not shown here) for cone shape gave an error of variance 0.050 for the shape factor computed using Req_{BL}.

Copyright © 2022 by author(s)

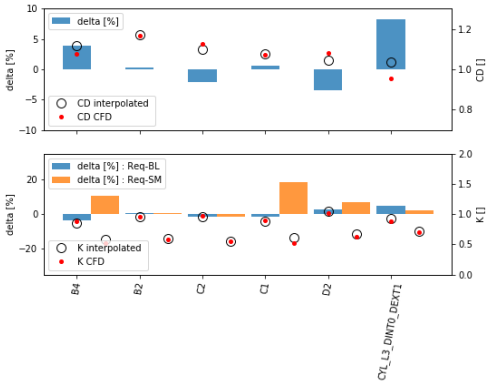

Fig. 17 : Leave one out on both QOI.

6. Conclusion

Formula to evaluate correlations – Eq. 1 and Eq. 2 – have been put to test with a large number of CFD computations with variations in modelling, TP and shape. Uncertainties related to CFD have been quantified and are sum up in Table 6. Using those formula, the drag coefficient and shape factor show limited variations when combined with the reference surface and the equivalent radius described here. The drag coefficient in tumbling has variations (for a fix shape) up to 5% between the chosen reference (laminar flow) and turbulent flow. And the variations from shape to shape can be up to 24%. The variations for the shape factor are larger. Turbulent flow and catalycity can play a significant effect depending on the condition but the primary source of variations is the geometry itself since the model show variations of shape factor up to 100% between the maximum and the minimum. A multi-linear interpolation of the QOIs from a database (build from CFD) depending on the non-dimensional parameters of shapes is helping to deal with the deviation of the QOIs from the normalized behavior (K=1.04 and CD=1.09). Such a database has been implemented in DEBRISK v3 [5]. This model is an improvement when compared to DEBRISK v2 [1], DRAMA [2] or ORSAT [3] that overestimate the risk because of the underestimation of the heat rate in the continuum regime [5].

The different uncertainties have been quantified with a relatively "low" number of computations and the geometry space could be explorer much further. Also, the effort to account for more detailed modelling such as the effect of turbulence or catalycity would be more significant. Nevertheless, the correlations from Eq. 1 and Eq. 2, Req, Sref as well as the value of CD and K taken from the database (and whose statistics are summed up Table 3) are a starting point to evaluate the drag and heat rate in tumbling of the corresponding shape. Finally, this work only covers the continuum regime but is beneficial to evaluate the QOIs in the transitional regime [12].

Acknowledgments

This work has been financed under contract n° 170990 from CNES.

References

1. Omaly P., Magnin Vella C., Galera S., "DEBRISK, CNES tool for re-entry survivability prediction: validation and sensitivity analysis", IAASS 2013, Montreal-Canada.
2. Kanzler R et al., "Upgrade of DRAMA's Spacecraft Entry Survival Analysis Codes", 4th International Workshop on Space Debris Reentry.
3. "Object Reentry Survival Analysis Tool (ORSAT) – Version 6.0. and its application to spacecraft entry", IAC-05-B6.3.06.
4. Klett R. D., "Drag Coefficients and Heating Ratios for Right Circular Cylinders in Free Molecular and Continuum Flow from Mach 10 to 30", SC-RR-64-2141, Sandia Corporation, Dec.1964.

Copyright © 2022 by author(s)

5. Annaloro J., Galera S., Thiebaut C., Omaly P., "Debrisk v3: new generation of object-oriented tools" 8th European Conference on Space Debris, ESA Space.
6. Detra R. W., Kemp, N. H., Riddell F. R., "Addendum to Heat Transfer to Satellite Vehicles Re-Entering the Atmosphere" Jet Propulsion, Vol. 27, No. 12, Dec. 1957, pp. 1256–1257.
7. Scott T et al., "MISTRAL: CONUS Debut Flow Field and Heat Transfer Calculations". 34th AIAA Fluid Dynamics Conference and Exhibit.
8. HTTPS://WWW.GRIDPRO.COM/
9. Annaloro J., Galera S., Thiebaut C., Spel M., Van Hauwaert P., Grossir G., Paris S., Chazot O., Omaly P., "Aerothermodynamics modelling of complex shapes in the DEBRISK atmospheric reentry tool: methodology and validation". IAC-19.A6.4.10x53828 (2019).
10. Meltzer B., "Shadow Area of Convex Bodies". Nature volume 163, page 220, 05 February 1949.
11. Albert J. Bushman Jr, Claud M. Pittman, "Configuration factor for exchange of radiant energy between axisymmetrical sections of cylinder, cones and hemispheres and their bases". NASA technical note D-944. Langley research center. October 1961.
12. Van Hauwaert P., "Approximation models for drag and heat flux of random tumbling objects in the transitional regime", HISST, 2022.

Annexes

Table 5 : Inflow conditions corresponding to trajectory points.

	TP1	**TP2**	**TP3**	**TP4**	**TP5**	**TP6**	**TP8**
Mach	10	15	10	9	15	20	5
Speed [m/s]	3013	4463	3013	2889	4770	5960	1599
Temperature [K]	225.85	220.25	225.85	256.26	250.61	220.1	251.1
Density [kg/m³]	1.14e-4	8.57e-5	1.14e-4	3.71e-3	3.64e-4	9.49e-5	0.00384
Temperature Wall [K]	1597	1095	799	700	700	700	1095
Modelling	Perfect gas / NE	Perfect gas / NE	Perfect gas	Perfect gas	NE	NE	Perfect gas
Molar fraction N2	0.79	0.79	-	-	0.767	0.767	-
Molar fraction O2	0.21	0.21	-	-	0.233	0.233	-

Copyright © 2022 by author(s)

Table 6 : Order or magnitude of the different uncertainties for the QOI in tumbling.

Variation	Reference, if applicable	Delta CD tumbling	Delta K tumbling	comments	Conservative with respect to the reference for risk assessment?
NE + fully (pseudo) catalytic	**Perfect gas**	+1%	+6%	Increase with flow enthalpy	Yes
Turbulent flow	**Laminar flow**	+5%	+15-20%	Turbulent flow depends on other parameters	K: Yes CD: No
Non catalytic wall	**Fully (pseudo) catalytic wall**	-	Up to -40%	Catalycity need to be accounted for.	No
Mesh convergence	**NA**	< +/-1%	< +/-3%		NA
Attitude discretization	**NA**	< +/-3%	< +/-4%	Average values are 1% for CD and 1.5% for K	NA
Invariance to inflow conditions	**NA**	< +/-4%	< +/-7%		NA
Geometry	**NA**	< +/-24%	< +/-100%	Not delta but ratio between max/min from Table 3	NA

Copyright © 2022 by author(s)

Table 7 : QOI in tumbling of selected shapes. Notation from **Fig. 1**

geometry	h [m]	DG [m]	e [m]	DP [m]	theta [m]	CD	K (Req=BL)
CYL_L3_DINT0_ DEXT1	3	1	0.5	1	360	0.956	0.886
ID3	0	4	0.003	0	360	1.08	0.702
ID6	0	4	0.96	0	45	1.035	1.108
ID9	0.1	6.8	0.003	6.8	360	1.121	0.98
ID11	0	7	0.003	6.8	360	1.16	0.982
ID13	0.1	6.896	0.048	6.896	360	1.056	0.866
ID14	0	7	0.048	6.8	45	1.113	0.901
C2	0.1351	6.0779	0.0113	6.0779	360	1.125	0.966
C1	0.855	8.5346	0.0158	8.5346	360	1.071	0.898
B2	0.1586	0.8903	0.0056	0.5972	360	1.169	0.952
B4	0.1077	5.1489	0.0445	3.753	360	1.078	0.877
D2	0.216	1.0802	0.0072	1.0802	360	1.083	1.022

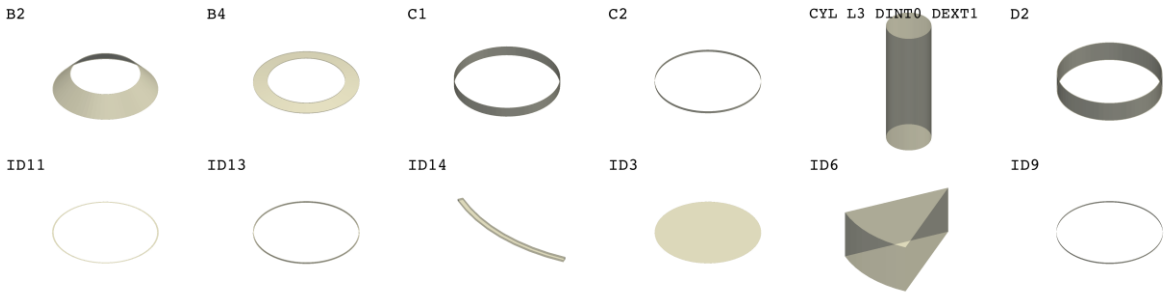

Fig. 18 : Drawing of the shape labelled in Table 7

Copyright © 2022 by author(s)